Karlsruher Institut für Technologie

Effect of torsion loading on swelling in silica

K.G. Schell, C. Bucharsky, T. Fett

KIT SCIENTIFIC WORKING PAPERS 154

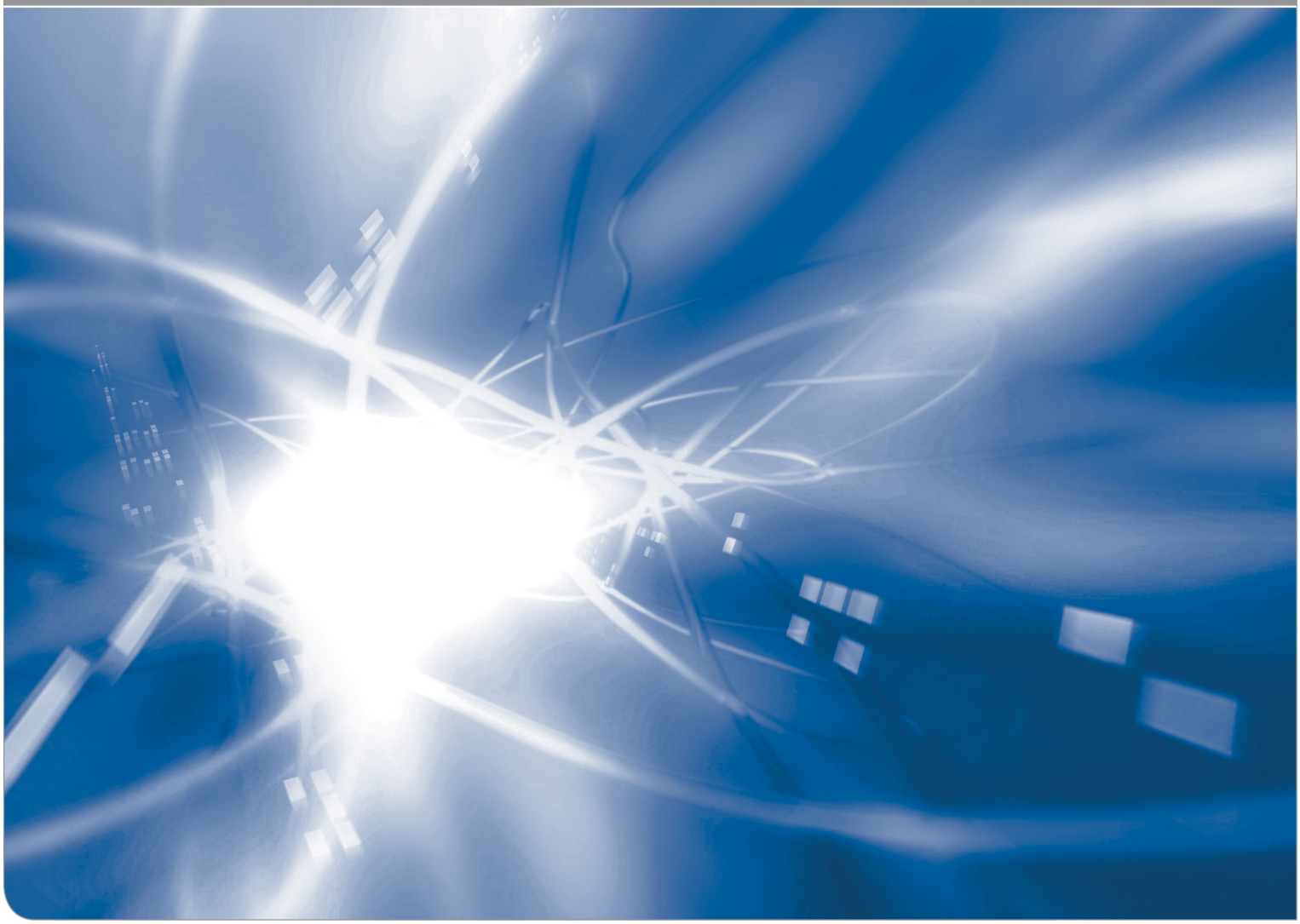

KIT – Universität des Landes Baden-Württemberg und nationales Forschungszentrum in der Helmholtz-Gemeinschaft

IAM Institute for Applied Materials

Impressum

Karlsruher Institut für Technologie (KIT)
www.kit.edu

2020

ISSN: 2194-1629

Abstract

Water reacting with silica causes the generation of hydroxyl SiOH accompanied by a volume or swelling expansion. The principle of LeChatelier ensures that the hydroxyl concentration increases with increasing externally applied stresses. From literature it becomes obvious that (a) the hydroxyl concentration must depend on the multi-axiality of the applied stresses, and (b) that the swelling effect is anisotropic. Based on Finite Element results it can be shown that for instance under torsion loading a strong stress-enhancement of the water/silica reaction with increased hydroxyl content must occur although this stress state shows a disappearing hydrostatic stress term.

Due to the disappearing hydrostatic stress term under torsion loading, no mechanical effect would have been expected in torsion tests. Seen from this point of view, the torsion test seems ideal to us to provide evidence of anisotropic swelling.

Further effects that can also influence the torsion test are addressed in the Appendix.

Contents

1. Torsion measurements from literature

Torsion tests on silica cylinders were performed by Aaldenberg et al. [1] at temperatures between 550°C and 700°C in normal lab air environment. The torsion moments M_t were measured as a function of time t for a constant drill angle as plotted in Fig. 1a. Different surface states were reached by grinding, polishing and flame-polishing. In Fig. 1b the results are plotted in the form

$$\Delta M_t(t) = M_t(t) - M_0 \tag{1.1}$$

vs $\sqrt{t}$, where M_0 is the moment at t=0. This report deals with the question of the fundamental effect of silica swelling by hydroxyl generation on twisted cylinder samples. In the Appendix, two other effects will be discussed qualitatively.

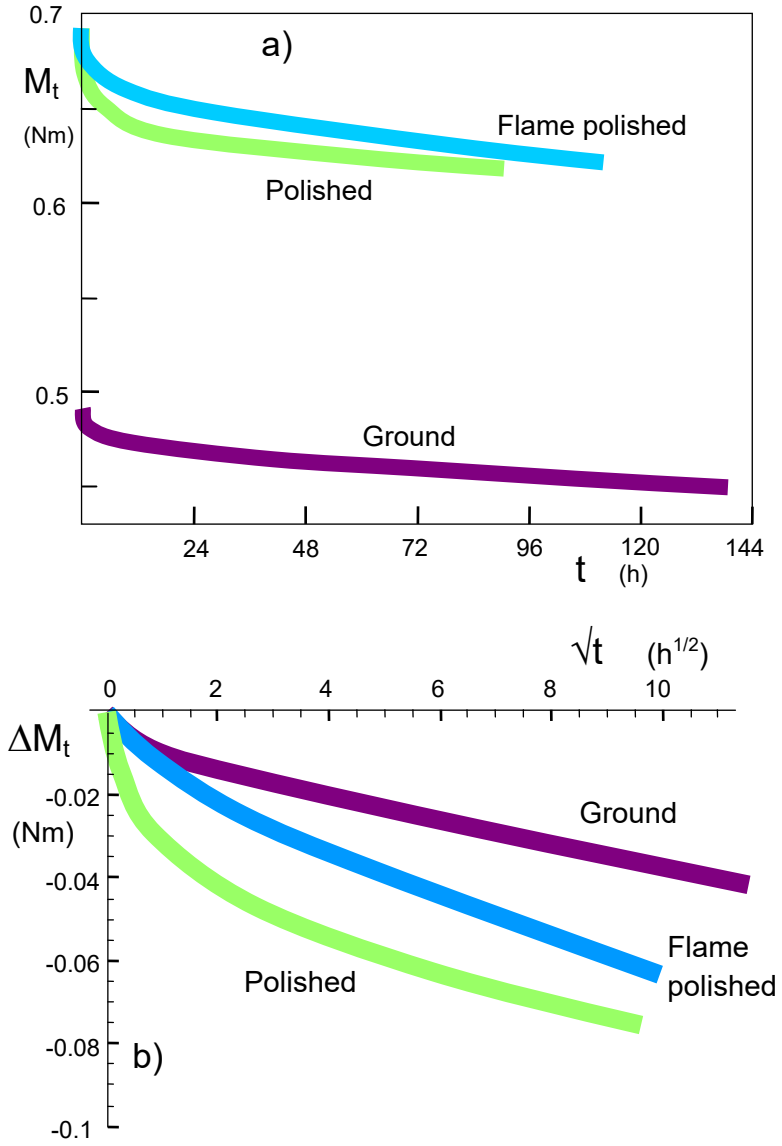

Fig. 1 Torsion measurements by Aldenberg et al. [1], a) torsion moment vs. time, b) change of the torsion moment vs. square-root of time.

2 Effect of swelling

2.1 Uniaxial tension

For uniaxial tension tests it holds for the stresses: $\sigma_z=\sigma_{appl}$, $\sigma_y=\sigma_x=0$ and for the swelling strains: $\varepsilon_{sw,y}=\varepsilon_{sw,x}$. The total swelling volume is in general the sum of the components

$$\varepsilon_v^{(z)} = \varepsilon_{sw,x} + \varepsilon_{sw,y} + \varepsilon_{sw,z} \tag{2.1}$$

with the superscript (z) indicates the direction of the uniaxial loading. The hydroxyl concentration reads

$$S = S_0 \exp\left[\sigma_z \frac{\Delta V}{RT} \right], \tag{2.2}$$

with an activation volume ΔV=14.4 cm^3/mol [2]. The swelling strain components were determined as

$$\varepsilon_{sw,z} = \alpha \varepsilon_v^{(z)} \tag{2.3}$$

with $\alpha\cong$1.92 [2], and

$$\varepsilon_{sw,x} = \varepsilon_{sw,y} = \tfrac{1}{2}(1-\alpha)\,\varepsilon_v^{(z)} \cong -0.46\,\varepsilon_v^{(z)} \tag{2.4}$$

The volume swelling strain $\varepsilon_v^{(z)}$ can be computed from the hydroxyl concentration S via [3]

$$\varepsilon_v^{(z)} = \kappa S,\ \kappa \cong 0.97 \tag{2.5}$$

For small stresses, eq.(2.2) can be linearized as

$$S = S_0(1+\sigma_z \frac{\Delta V}{RT}), \tag{2.6a}$$

$$\varepsilon_v^{(z)} = \varepsilon_{v,0}(1+\sigma_z \frac{\Delta V}{RT}), \tag{2.6b}$$

where $\varepsilon_{v,0}$ is the volume swelling in the absence of an applied stress. A continuous first derivative with respect to the stress at the origin is assumed.

The increase of the volume swelling strain due to the load may be denoted as

$$\Delta\varepsilon_v^{(z)} = \varepsilon_{v,0}\,\sigma_z \frac{\Delta V}{RT}, \tag{2.7}$$

and the linear strains as

$$\Delta\varepsilon_{sw,z} = \alpha \Delta\varepsilon_v^{(z)} \tag{2.8}$$

$$\Delta\varepsilon_{sw,x} = \Delta\varepsilon_{sw,y} = \tfrac{1}{2}(1-\alpha)\,\Delta\varepsilon_v^{(z)} \cong -0.46\,\Delta\varepsilon_v^{(z)} \tag{2.9}$$

2.2 Torsion loading

Under torsion loading, the maximum and minimum principal stresses appear in a coordinate system turned by 45° with respect to the length axis. In this system, Fig. 2, the “applied” stresses are

$$\sigma_{appl,y} = -\sigma_{appl,z}\ ,\quad \sigma_{appl,x} = 0 \tag{2.10}$$

This loading case can be simply handled by superposition of uniaxial tensile and uniaxial compression tests. By renaming the coordinates, the stress $\sigma_{app,y}$ causes the swelling strains

$$\Delta\varepsilon_v^{(y)} = \varepsilon_{v,0}\,\sigma_y\,\frac{\Delta V}{RT} = -\varepsilon_{v,0}\,\sigma_z\,\frac{\Delta V}{RT}, \tag{2.11}$$

where now the superscript (y) stands for loading in y-direction. The other swelling strain components are

$$\Delta\varepsilon_{sw,y} = \alpha\,\Delta\varepsilon_v^{(y)} \tag{2.12}$$

$$\Delta\varepsilon_{sw,x} = \Delta\varepsilon_{sw,z} = \tfrac{1}{2}(1-\alpha)\,\Delta\varepsilon_v^{(y)} \cong -0.46\,\Delta\varepsilon_v^{(y)} = 0.46\,\Delta\varepsilon_v^{(z)} \tag{2.13}$$

By superimposing the individual strains to the total ones (indicated by subscript "tot") it results

$$\Delta\varepsilon_{v,tot} = 0, \tag{2.14}$$

$$\Delta\varepsilon_{sw,x,tot} = 0 \tag{2.15}$$

$$\Delta\varepsilon_{sw,z,tot} = \varepsilon_{v,0}\,\sigma_z\,\frac{\Delta V}{RT}\left(\tfrac{3}{2}\alpha - \tfrac{1}{2}\right) \cong 2.38\,\varepsilon_{v,0}\,\sigma_z\,\frac{\Delta V}{RT} \tag{2.16}$$

$$\Delta\varepsilon_{sw,y,tot} = -\Delta\varepsilon_{sw,z,tot} \tag{2.17}$$

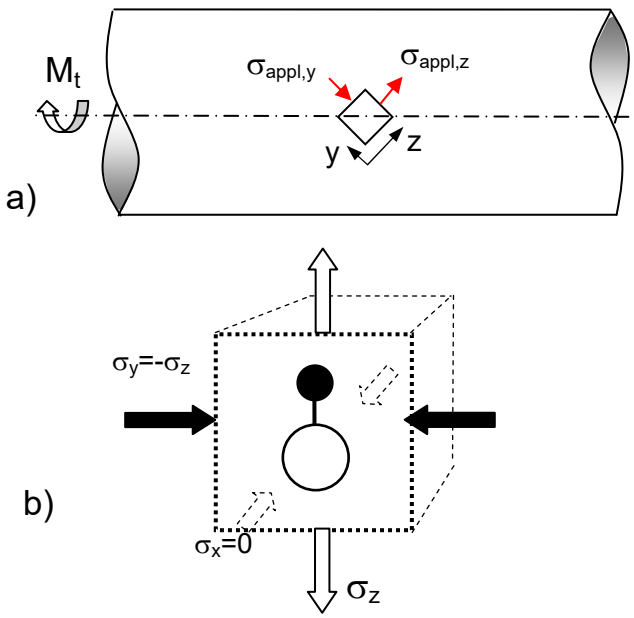

Fig. 2 a) Cylinder under torsion moment M_t, b) applied stresses in the principal axes system shown on a volume element with a schematic representation of a Si-O bond.

2.3 Swelling stresses

Since in water diffusion layers the swelling strains are present only in thin surface layers, free expansion is not possible due to the bulk material that remains free of water. In the surface layer, swelling strains are created causing swelling stresses $\sigma_{sw,z}$ and $\sigma_{sw,y}$.

Due to the compatibility condition between surface layer and bulk, the total strains consisting of elastic and swelling strains, must be the same in the layer as in the bulk material.
This condition can be expressed as

$$\Delta\varepsilon_z = \Delta\varepsilon_{sw,z} + \frac{\Delta\sigma_{sw,z,tot}}{E} - \nu\frac{\Delta\sigma_{sw,y,tot}}{E} - \underbrace{\nu\frac{\Delta\sigma_{sw,x,tot}}{E}}_{=0} = 0 \tag{2.18}$$

$$\Delta\varepsilon_y = -\Delta\varepsilon_{sw,z,tot} + \frac{\Delta\sigma_{sw,y,tot}}{E} - \nu\frac{\Delta\sigma_{sw,z,tot}}{E} - \underbrace{\nu\frac{\Delta\sigma_{sw,x,tot}}{E}}_{=0} = 0 \tag{2.19}$$

The solution of this system of linear equations reads

$$\Delta\sigma_{sw,z,tot} = -\frac{E}{1+\nu}\Delta\varepsilon_{sw,z,tot} \tag{2.20}$$

$$\Delta\sigma_{sw,y,tot} = \frac{E}{1+\nu}\Delta\varepsilon_{sw,z,tot} \tag{2.21}$$

These two swelling stresses cause a shear stress

$$\Delta\tau_{sw} = \tfrac{1}{2}(\Delta\sigma_{sw,z,tot} - \Delta\sigma_{sw,y,tot}) = -\frac{E}{1+\nu}\Delta\varepsilon_{sw,z,tot} \tag{2.22}$$

Here E is Young's modulus and ν Poisson's ratio (E=72000 MPa, ν=0.17).
In terms of the applied torsion stress

$$\tau_{appl} = \tfrac{1}{2}(\sigma_z - \sigma_y) = \sigma_z \tag{2.23}$$

it finally holds by use of the proportionality eq.(2.5),

$$\Delta\tau_{sw} = -\frac{E}{1+\nu}\kappa S_0\,\tau_{appl}\frac{\Delta V}{RT}(\tfrac{3}{2}\alpha - \tfrac{1}{2}) \tag{2.24}$$

This shear stress acts against the externally applied torsion.

2.4 Swelling moment

The change of torsion moment caused by swelling in a thin surface layer of thickness b that is small compared to the cylinder radius R of the test specimen, $b \ll R$, is given as

$$\Delta M_{t,sw} \cong \Delta\tau_{sw} \times \underbrace{2\pi R b}_{\text{Water-affeted area}} \times \underbrace{R}_{\text{"Cantilever arm"}} \tag{2.25}$$

The water diffusion layer b increases with time t according to

$$b = \sqrt{D_{eff}\,t} \tag{2.26}$$

where D is the diffusivity. The swelling moment can, therefore, be expressed by

$$\Delta M_{t,sw} = -\frac{\pi E}{1+\nu}\kappa\frac{\Delta V\,\tau_{appl}}{RT}(3\alpha - 1)R^2\sqrt{t}\,S_0\sqrt{D_{eff}} \tag{2.27}$$

3 Effect of the damage-affected modulus

A second influence of the water penetrating into the surface is the damage of the original material by hydroxide formation interrupting the ring structure of silica.

In damage mechanics according to Lemaitre [4], the damage variable D represents the part of the material cross-section that can no longer transmit forces. As outlined in [5], the area that can carry load, A_D, is reduced to

$$A_D = A_0(1-D) \tag{3.1}$$

where A_0 denotes the total geometrical cross section subsuming damaged and undamaged regions. According to the hypothesis of strain equivalence by Lemaitre [4], the effective elastic modulus of the damaged glass, E_D, decreases with increasing damage

$$E_D = E_0(1-D) \tag{3.2}$$

where E_0 is the modulus of the virgin glass. For small hydroxyl concentrations it can be written

$$D(S) = \lambda S \tag{3.3}$$

with $\lambda \approx 10.6$ [6, 7]. For not too large damage ($D<0.5$) the Poisson's ratio doesn't change more than 10% and can for our purpose assumed as a constant [8]. Then eq.(3.2) holds also for the shear modulus G_D

$$G_D = G_0(1-D) \tag{3.4}$$

In a strain- or displacement-controlled test, the decrease of the stresses in the damaged zone, σ_D, τ_D, are then

$$\frac{\sigma_D}{\sigma_0} = \frac{\tau_D}{\tau_0} = (1-D) \tag{3.5}$$

with the original stresses σ_0 and τ_0 in the surface region. Consequently, the decrease of the torsion moment is for thin layers $b<<R$

$$\Delta M_{t,D} = 2\pi R^2(\tau_D - \tau_0)\, b = -2\pi R^2 \tau_0\, D\, b = -2\pi R^2 \tau_0 \lambda \sqrt{t}\, S_0 \sqrt{D_{eff}} \tag{3.6}$$

where the subscript "D" indicates the change due to damage. The ratio of the two moments is

$$\frac{\Delta M_{t,sw}}{\Delta M_{t,D}} = \frac{(3\alpha - 1) E \kappa \Delta V}{2\lambda(1+\nu) RT} \tag{3.7}$$

At 700°C, this ratio is about 24, i.e. the dominant effect of hydroxyle generation on the torsion moment is via swelling. Finally, the total change caused by the two effects is

$$\Rightarrow \Delta M_t = -\left(\frac{E}{1+\nu} \kappa \frac{\Delta V}{RT} (3\alpha - 1) + 2\lambda \right) \pi R^2 \tau_{appl} \sqrt{t}\ \underbrace{S_0 \sqrt{D_{eff}}}_{\eta} \tag{3.8}$$

where the parameter $\eta=S_0\sqrt{D}$ depends on the material, the environment, and the temperature. The paper of Aaldenberg et al. [1] doesn't provide any information on D_{eff} and the surface water concentration S_0, which was probably not measured. Consequently, the quantity η has to be used here as an unknown parameter.

4. Application to torsion experiments by Aaldenberg et al. [1]

Figure 3 shows again the results of Fig. 1b plotted vs. the square root of time. The red straight lines represent the behavior for long times. The slopes of these asymptotes are listed in Table 1. Whereas the slopes for the ground and the polished specimens are almost identical, the slope of the flame-polished material is steeper. The related parameter $\eta=S_0\sqrt{D}$ is given in the third Column of Table 1.

Surface state	Slope (Nm/s$^{1/2}$)	Parameter $\eta=S_0\sqrt{D_{eff}}$ (m/$\sqrt{s}$)
ground	-1.60×10^{-4}	1.06×10^{-9}
polished	-1.75×10^{-4}	1.17×10^{-9}
flame-polished	-2.53×10^{-4}	1.70×10^{-9}

Table 1 Parameter η according to eq.(3.8) from straight-line evaluation of Fig. 3.

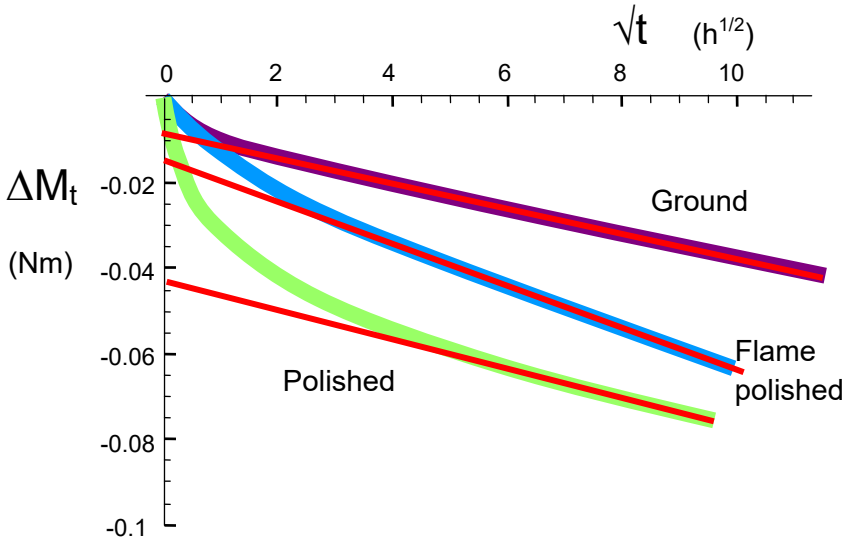

Fig. 3 Data by Aaldenberg et al. [1] for 700°C given in Fig. 1b, straight lines indicate linear long-time behaviour.

5. Discussion

From Figs. 1 and 3 there are strong deviations from the straight-line behaviour visible for short times. The moment decreases much faster. In our opinion there are two effects responsible for this behaviour:

5.1 Origin for the time *t*

In [1] it is mentioned that for heating up the furnace to test temperature a time "on the order of one hour" was necessary. During this pre-heating time, the test specimen was already mounted in the test apparatus. Especially in the time span where the test temperature was nearly reached, the diffusion zone could already grow with high growth velocity due to the square-root dependence $b \propto \sqrt{t}$. Consequently, the time origin for the growth of the water diffusion zone is different from the time under load. The effect is illustrated in Fig. 4 for the ground and the flame-polished specimens which show clear straight-line behaviour over a large time span. The time origin for diffusion, here t', is shifted by 1 hour, i.e. $t'=t+1\text{h}$. This effect is trivially more significant for small times and can be neglected for large times. About 35-40% of the early deviations would rise from the origin shift by 1h.

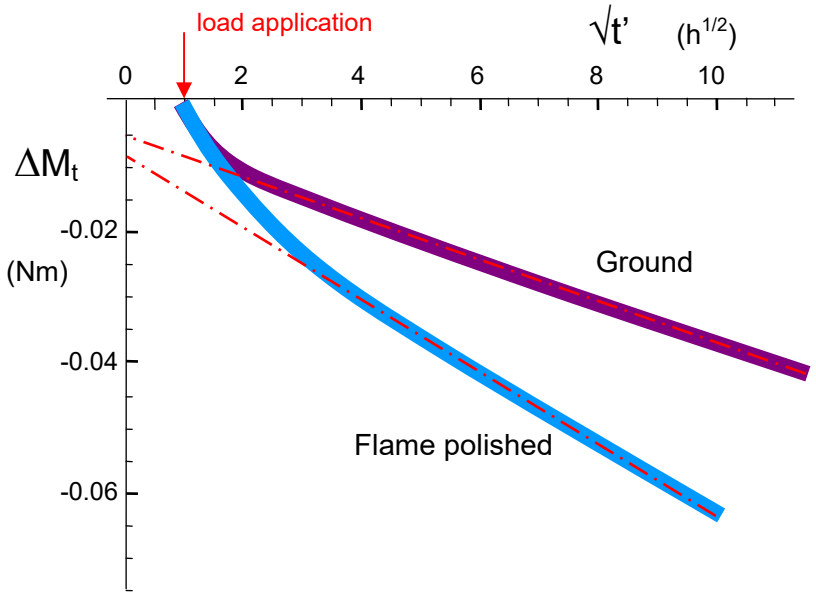

Fig. 4 Data from Fig.3, plotted vs the time t' for diffusion, by use of $t'=t+1\text{h}$.

5.2 Effect of surface cracks

In ground silica surfaces cracks are present as has been outlined by Suratwala et al. [9]. Even in the case of finishing by mechanical polishing or chemical etching larger cracks remain if the additionally removed surface layer is less than the crack depths after grinding. The individual distributions of the depths a and the widths L are approximated in [9] by exponential distribution function

In [10] we computed an apparent thickness b_{app} of the diffusion zone for the case of a surface containing many small machining cracks. When these cracks are modelled as an array of edge cracks of depth a, schematically illustrated by Fig. 5a, the water can penetrate into the glass through the undamaged surface $L \times B$ and through the crack faces $L \times a$, (L= length of the surface element). At very short times the volume V of water entrance into a single array element comes from the specimen surface $V_s = L \times B \times b$ *and* the two crack faces $V_c = L \times a \times b$ with b given by eq.(2.26). For small layer thickness, $b << (a, B/2)$, the apparent layer thickness b_{app} can be defined as

$$b_{app} = b\left(1+\frac{2a}{B}\right), \text{ for } b \to 0 \tag{5.1}$$

For large layer thickness, $b>>a$,

$$b_{app} \to b \ , \text{ for } b \to \infty \tag{5.2}$$

These two limit dependencies may be interpolated by a continous dependency

$$b_{app} \approx b\left(1+\frac{2a}{B}\exp\left[-\frac{b}{\min[a,\frac{1}{2}B]}\right]\right) \tag{5.3}$$

or more general by introducing a fitting parameter χ

$$b_{app} \cong b\left(1+\frac{2a}{B}\exp(-\chi\, b/a)\right) \tag{5.4}$$

where a and B are average values of crack depth and crack spacing. Figure 5b shows the apparent zone depth by eq.(5.4) for χ=1. Since the change of the torsion moment is negative, $-b_{app}$ is plotted.

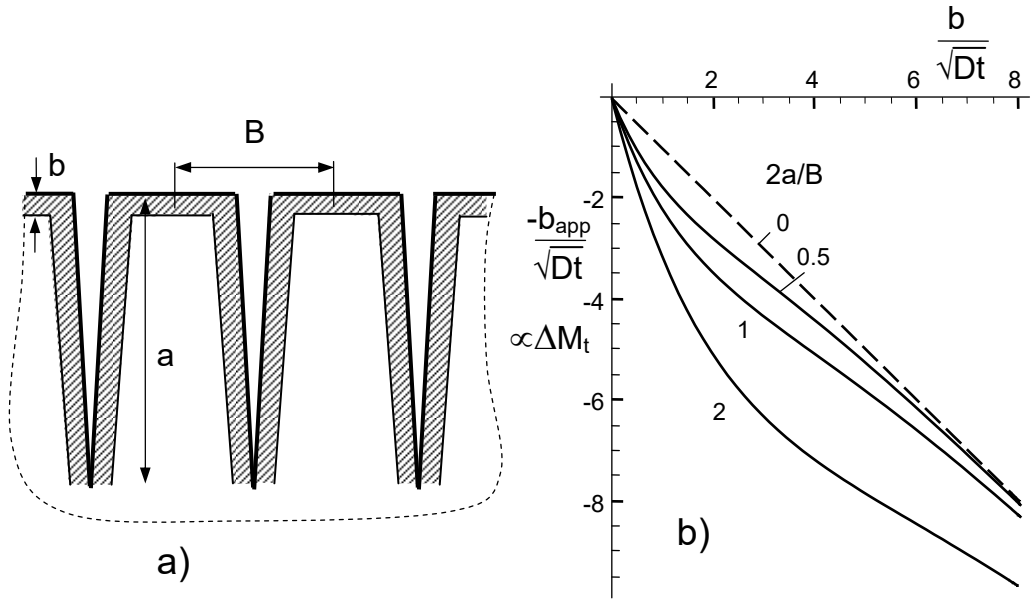

Fig. 5 a) Surface cracks due to surface treatment, modelled by an array of periodical edge cracks, b) apparent diffusion layer thickness b_{app} as a function of the true layer thickness b for several parameters a/B and χ=1.

Final Remark: Due to the disappearing hydrostatic stress term under torsion loading, no mechanical effect would have been expected in torsion tests. Seen from this point of view, the torsion test seems ideal to us to provide evidence of anisotropic swelling.

APPENDIX

A1 Hydroxyl concentration at high temperature

A1.1 Diffusivity

When water diffuses into silica glass, it reacts with the silica network according to the following equation:

$$\equiv\text{Si-O-Si}\equiv + \text{H}_2\text{O} \leftrightarrow \equiv\text{SiOH+HOSi}\equiv, \tag{A1.1}$$

with the molar concentration of hydroxyl groups, $S = [\equiv\text{SiOH}]$, and the molar concentration of water, $C = [\text{H}_2\text{O}]$. For reaction of Eq. (A1.1), the equilibrium constant is at high temperatures ≥ 450°C

$$K = \frac{S^2}{C} \tag{A1.2}$$

In this case, the hydroxyl groups are mobile and can move away from one another; they become independent, and the reverse reaction behaves as a normal bimolecular reaction. In the high-temperature region, $T \geq 450$°C, the OH groups must be mobile and show a minimum diffusivity in order to sample neighboring OH groups, leading to a bimolecular reverse reaction, as has been required by Doremus [11]. His estimation for the minimum hydroxyl diffusivity, D_{OH}, was

$$D_{\text{OH}} \geq 10^{-17}\ \text{cm}^2/\text{s} \tag{A1.3}$$

In the preceding considerations we only considered the effective diffusivity that is based on the diffusion of molecular water including the reaction (A1.1).

Water near a crack tip can enter the material easier due to enhanced diffusivity D under mechanical load according to [12]

$$D = D_0 \exp\left[\sigma_h \frac{\Delta V}{RT}\right] \tag{A1.4}$$

where D_0 denotes the value of the diffusivity in the absence of a stress. T is the absolute temperature in K; $\Delta V \approx 15\ \text{cm}^3/\text{mol}$ is the activation volume for stress-enhanced diffusion and R is the universal gas constant.

The diffusivity of the OH-groups, $D_S = D_{\text{OH}}$, from Yongheng and Zhenan [14] is plotted in Fig. 6 together with the effective diffusivity D_{eff} according to Davis and Tomozawa [13]. For the case of a partial water vapor pressure of 6 Torr representing normal lab air, the diffusivities by Davis and Tomozawa were transformed from the data at 355 Torr via

$$D_{6\,\text{Torr}} = D_{355\,\text{Torr}} \sqrt{\frac{6\,\text{Torr}}{355\,\text{Torr}}} \tag{A1.5}$$

The straight lines in Fig. 6 can be represented by

$$D_S = D_0 \exp\left(\frac{-Q_s}{RT}\right) \tag{A1.6a}$$

with D_0=1010 cm^2/s and Q_S=261 kJ/mol (red line). The effective diffusivities from [13] may be described by

$$D_{eff} = D_{eff,0} \exp\left(\frac{-Q_{eff}}{RT}\right) \tag{A1.6b}$$

with $D_{eff,0}$=1.2 10^{-6} cm^2/s at 355 Torr and Q_{eff}=80.6 kJ/mol .

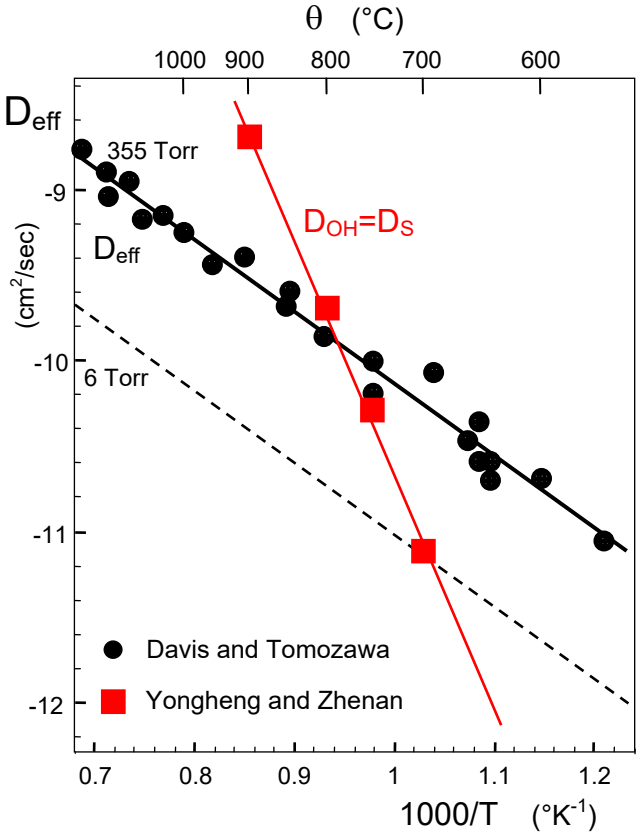

Fig. 6 Arrhenius plot of diffusivities, black: effective water diffusivity in silica at 355Torr by Davis and Tomozawa [13], red: diffusivity of hydroxyls from dehydroxylation experiments by Yongheng and Zhenan [14].

A1.2 Hydroxyl generation at crack tips

In ground silica surfaces cracks are present even in the case of finishing by mechanical polishing or chemical etching. This has been outlined by Suratwala et al. [9]. Such a surface state is schematically shown in Fig. 7 in side- and front view. The individual distributions of the depths a and the widths L are approximated in [9] by exponential distribution function.

When a mechanical tensile stress σ is applied (Fig. 7), 50% of all surface cracks are oriented normally to the stress direction in a statistical sense. Such cracks will be considered in the following computations.

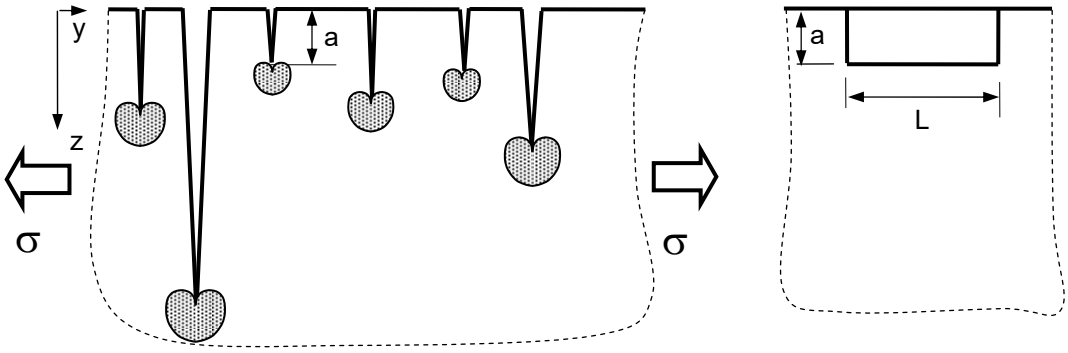

Fig. 7 Stress-enhaced hydroxyl generation at the tips of surface cracks under load.

A2 An alternate scenario for the decreasing torsion moment

When silica surfaces undergo high-temperature treatment in lab air, they are strongly damaged as can be concluded from strength measurements on silica fibers by Proctor et al. [15]. Surface inspections after the strength tests revealed the local damages from which final fracture started. An example of such a surface damage for a heat-treatment time of 30-40 min at 800°C in lab air is shown in Fig. 8. From this image and the crack-face view in [15] we can conclude that the corrosion events appear roughly as a hemisphere that is strongly cracked by irregularly orientated cracks. From the two images, the radius ρ of the damages was determined as given in Table 2. For the torsion tests at 700°C we have to expect about ρ≈14 μm after t=30-45 min.

Proctor et al. [15] explain the damage events as dust contamination that reacts with the silica surface. The nature of the atmosphere should have a small effect. This conclusion is drawn from the fact that the strength in vacuum is only slightly increased and only the dust particles already deposited on the surface become effective. The damaged zone in Fig. 8 is strongly cracked by irregularly orientated cracks. This region cannot carry external load. From a mechanics point of view it can be modelled as a hemisphere with a disappearing Young's modulus, E≅0.

Temperature	ρ (μm)
600°C	7.6
800°C	22.4

Table 2 Radii for semi-spherical pores reported by Proctor et al. [15].

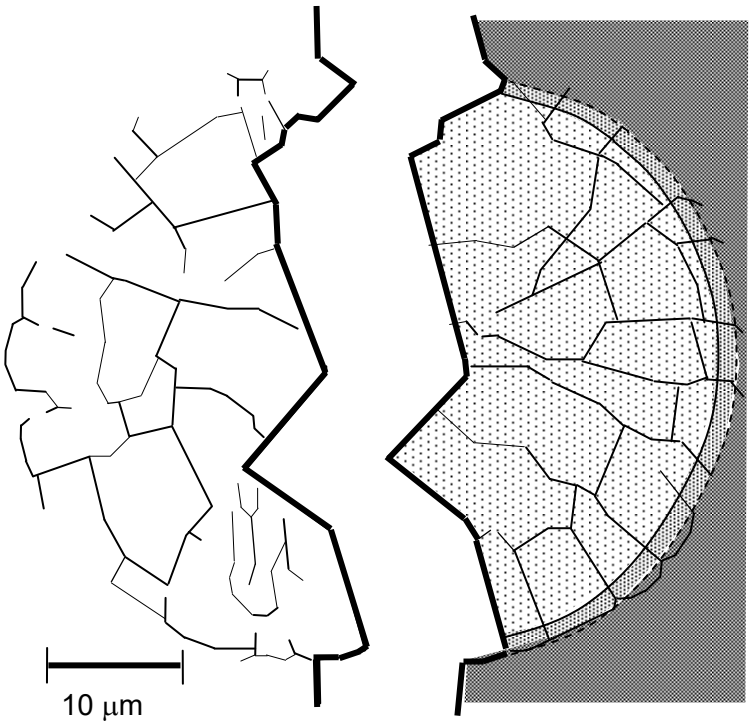

Fig. 8 Crack patterns within a nearly spherical surface damage according to Proctor et al. [15], left part: Cracks exclusively, right part: Shadowing included.

For an estimation of the surface damages on the reduction of the cross-section let us consider a part of the specimen surface with a length L in axial direction. When N damages are in a surface area $A=2\pi RL$, the damage density is $n=N/2\pi RL$. The average damage radius $\overline{\rho}$ for a number of N damages may be defined via the volume of the N damages of not necessarily identical radii per surface area is

$$\overline{\rho} = \left(\frac{1}{N} \sum_{i=1}^{N} \rho_i^3 \right)^{1/3} \tag{A2.1}$$

When N damages are in the unit surface area A, the damage density is $n_A=N/A$. The damage volume is

$$V / A = n_A \tfrac{2}{3} \pi \overline{\rho}^3 \tag{A2.2}$$

This volume through which no load can be transmitted corresponds to an effective reduction in the cylinder radius, b, of

$$b = \frac{V}{A} \tag{A2.3}$$

as indicated in Fig. 9. The change of torsion moment caused by surface damaging is again given by

$$\Delta M_t \cong -\tau \times \underbrace{2\pi R b}_{\substack{\text{damaged} \\ \text{cross section}}} \times \underbrace{R}_{\text{"Cantilever arm"}}$$

The effective radius reduction depends on time, b=f(t), because of

- The increased number of damage events which is proportional to time t as long as no interactions between the damages occur and older damages interfere with newer dust particles.
- The reaction rate between the dust particles and the silica surface is limited and dust contamination and silica need time for reaction.

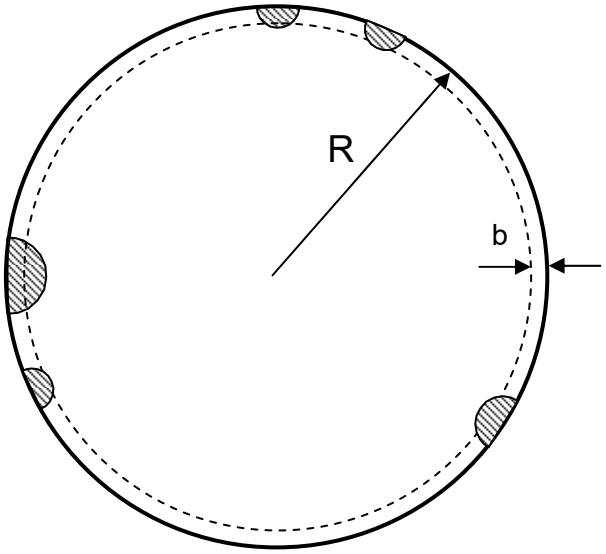

Fig. 9 Stress-free surface region due to surface damages (schematic).

References

1 Aaldenberg EM, Aaldenberg JS, Blanchet TA, Tomozawa M. Surface shear stress relaxation of silica glass. J Am Ceram Soc. 2019;00:1-10. https:doi.org/10.1111/jace.16342

2 S. M. Wiederhorn, G. Rizzi, S. Wagner, M. J. Hoffmann, T. Fett, Stress-Enhanced Swelling of Silica: Effect on Strength, J. Am. Ceram. Soc. **99**(2016), 2956-63

3 S. M. Wiederhorn, F. Yi, D. LaVan, T. Fett, M.J. Hoffmann, Volume Expansion caused by Water Penetration into Silica Glass, J. Am. Ceram. Soc. **98** (2015), 78-87.

4 Lemaitre J. How to use damage mechanics. *Nuclear Eng Design.* 1984;80:233-245.

5 T. Fett, K. G. Schell, M. J. Hoffmann, S. M. Wiederhorn, Effect of damage by hydroxyl generation on strength of silica fibers, J Am. Ceram Soc. 2018;**101**:2724–2726.

6 T. Fett, G. Schell, Consequence of Damage in Silica on Young's Modulus, **51**, 2017, ISSN: 2194-1629, Karlsruhe, KIT.

7 K.G. Schell, T. Fett, C. Bucharsky, M.J. Hoffmann, S.M. Wiederhorn, Damage by Hydroxyl Generation in Silica, Glass Physics and Chemistry, **46**(2020), 424-428.

8 D. Ashkin, R.A. Haber, J.B. Wachtman, Elastic properties of porous silica derived from colloidal gels, J. Am. Ceram. Soc., **73**(1990), 3376-81.

9 T. Suratwala, L. Wong P. Miller, M.D. Feit, J. Menapace, R. Steele, P. Davis, D. Walmer, Sub-surface mechanical damage distributions during grinding of fused silica, J. Non-Cryst. Solids, **352**(2006), 5601-5617.

10 T. Fett, G. Schell, Water diffusion in cracked surface layers – unloaded cracks, **124**, 2019, ISSN: 2194-1629, Karlsruhe, KIT.

11 R.H. Doremus, Diffusion of water in silica, J. Mat. Res. **10**(1995), 2379-89.

12 P.G. Shewman, Diffusion in Solids, McGraw-Hill, New York, 1963.

13 Davis, K.M., Tomozawa, M., Water diffusion into silica glass: structural changes in silica glass and their effect on water solubility and diffusivity, J. Non-Cryst. Sol. **185** (1995), 203-220.

14 Z. Yongheng, G. Zhenan, The study of removing hydroxyl from silica glass, J. Non-Cryst. Solids, **352**(2006), 4030-4033.

15 A. Proctor, I. Whitney, J.W. Johnson, The strength of fused silica, Proceedings of the Royal Society of London. Series A. Mathematical and Physical Sciences, Vol. 297, No. 1451 (1967), 534-557.

KIT Scientific Working Papers
ISSN 2194-1629

www.kit.edu